Multiple scattering in the Compton effect. III. Monte Carlo calculations

Anthony C. Tanner and Irving R. Epstein*
Department of Chemistry, Brandeis University, Waltham, Massachusetts 02154
(Received 24 November 1975)

Total probabilities, angular distributions, and energy profiles of multiply scattered radiation are calculated using Monte Carlo techniques. It is found that use of either the Klein-Nishina or the polarization-dependent Thomson cross section can result in significant departures from the angular distributions and energy profiles obtained with the polarization-averaged Thomson cross section. The radius of the incident photon beam appears to have a substantial influence on multiple scattering probabilities and angular distributions for finite cylindrical samples. Criteria are established for estimating under what experimental conditions a sample may be considered effectively "infinite," so that earlier analytic results become applicable. Triple and higher-order scattering are found to be generally insignificant for finite cylinders.

I. INTRODUCTION

A. Preliminary remarks

In the two previous papers of this series[1,2] (hereafter referred to as I and II) we treated the problem of multiple scattering in a typical Compton experiment analytically or semianalytically by introducing a somewhat simplified model of the experimental situation. The advantages of such a treatment are as follows: (a) The results obtained are exact or nearly exact within the limitations of the model; (b) the calculations lay bare some of the more important variables in the experiment, thereby making it possible to develop intuitions which can, hopefully, be extrapolated to more complicated systems; and (c) because of (a) and the fact that an analytic expression is obtained, it is possible to quantitatively assess the relative importance of changes in the variables referred to in (b). For example, in I and II we were able to evaluate the effect on angular distributions and energy profiles, respectively, of employing different forms for the scattering cross section.

As we noted in I and II, some of the analytic results obtained there may in fact be applicable to actual experiments, if the attenuation coefficient and sample geometry are such that the sample may be viewed as an infinite slab or cylinder. However, for a wide range of experiments such conditions are *not* met, and the extent and effect of multiple scattering are then best calculated by Monte Carlo techniques.

A number of such calculations have already been performed, the most relevant to Compton experimentalists being those of Felsteiner *et al.*[3-5] and of Williams and Halonen.[6,7] The latter investigators, in particular, have developed a highly efficient Monte Carlo program which realistically accounts for a number of phenomena present in an actual experiment, such as binding-energy cutoffs for inner-shell electrons, variation of the shape of the energy profile with sample thickness, and realistic electron momentum distributions.

In this paper, we again restrict our calculations to simpler models than those considered by other workers. Their main interest has been in minimizing the amount of multiple scattering or in correcting experimental profiles for its effects. We, too, shall consider these problems in a fourth paper in this series. Here, however, we employ the Monte Carlo approach primarily to assess the approximations of I and II.

B. Statement of the general problem

Before concluding the Introduction, we think it useful to present a mathematical description of a rather realistic model of a Compton scattering experiment. While our formulation will be totally beyond exact solution, it will enable our work as well as that of others to be easily described and classified as subcases of the more general problem.

Multiple scattering in Compton experiments is an example of the exceedingly complicated problem of the transport of high-energy particles in matter.[8,9] Fortunately, in the domain of energies usually involved in Compton experiments (~0.01–0.2 MeV) only three processes are at all probable, their relative importance depending upon initial energy and sample composition.[10] These processes are (a) Compton (inelastic) scattering; (b) Rayleigh (elastic) scattering, including coherent scattering at small angles; and (c) photoelectric absorption.

Let us define the following quantities for the above processes for some energy E:

(i) $\mu_c(E)$ is the linear attenuation coefficient for Compton scattering from bound electrons in the sample, i.e., the fraction of photons Compton scattered on passing through a thickness dl is

$-dn/n = \mu_c(E)\,dl$.

(ii) $\mu_R(E)$ is the coefficient for Rayleigh scattering including coherent scattering.

(iii) $\mu_\tau(E)$ is the photoelectric absorption coefficient.

(iv) $\mu(E) \equiv \mu_c(E) + \mu_R(E) + \mu_\tau(E)$, the total attenuation coefficient. All attenuation coefficients are in cm^{-1}.

(v) $f_i(E) = \mu_i(E)/\mu(E)$, the probability that a collision with an electron will be a Compton ($i = C$), Rayleigh ($i = R$), or photoelectric ($i = \tau$) event.

Consider a cylindrical sample of thickness t and radius R_f as shown in Fig. 1. An arbitrary point within the cylinder is described by a vector $\vec{\rho}$ [e.g., $\vec{\rho} = (r_c, \gamma_c, z)$ or $\vec{\rho} = (x, y, z)$]. The cylinder is irradiated by a beam of photons. The direction of the photon beam is given by a unit direction vector $\vec{k}_b$, but we allow for the possibility of a distribution of initial photon directions $\vec{k}_0$ about $\vec{k}_b$. We also assume a distribution of initial photon energies E_0 around some most probable value $\bar{E}_0$. Let $\Delta(\vec{k}_0, E_0)$ be this distribution of initial photon directions and energies. An incident photon is thus described by $E_0, \vec{k}_0$ and r_b, γ_b, its position in the photon beam (Fig. 1). We require that a photon with $r_b = 0$ and $\vec{k}_0 = \vec{k}_b$ impinge on the sample at $r = 0$. The total incident photon flux is just

$$I_{\text{tot}} = \int_{\text{all } \vec{k}_0} d\vec{k}_0 \int_{E_0^{\min}}^{E_0^{\max}} dE_0 \Delta(\vec{k}_0, E_0) \times \int_0^{2\pi} d\gamma_b \frac{1}{2\pi} \int_0^{R_b} dr_b \frac{2r_b}{R_b^2}.$$

Now consider a photon with fixed $\vec{k}_0$ and E_0, and let us define a double scattering event by an ordered pair (A_1, A_2), where $A_i = C$ if a scattering is Compton and $A_i = R$ if it is Rayleigh. Define $l_0(\vec{k}_0, \vec{\rho}_0)$ as the path length from the point of entry $\vec{\rho}_0$ on the cylinder face to the cylinder boundary along $\vec{k}_0$. Suppose that the photon scatters within the sample at a point $\vec{\rho}_1$ from an electron with momentum $\vec{p}_1$. Let $l_0' = |\vec{\rho}_1 - \vec{\rho}_0|$. Clearly $l_0' \le l_0$. The probability distribution for the new scattering direction $\vec{k}_1$ is given by the differential scattering law $(d\sigma/d\Omega)_A$. Let $\mu_0\,[= \mu_0(E_0)]$ be the initial total attenuation coefficient and $f_{0,A_1}[= f_{0,A_1}(E_0)]$ be the probability that the first collision is of type A_1. Let $l_1 = l_1(\vec{k}_1, \vec{\rho}_1)$ be the path length from $\vec{\rho}_1$ to the cylinder boundary along $\vec{k}_1$. The new attenuation coefficient μ_1 depends upon the energy of the scattered photon, which is given by the Compton equation

$$\frac{1}{E_1} = \frac{1}{E_0} + 2\sin^2\left(\frac{\theta_1}{2}\right) + \left(\frac{2}{E_0}\right)\left(\frac{\bar{p}_1}{137}\right)\sin\left(\frac{\theta_1}{2}\right), \qquad (1)$$

where the scattering angle θ_1 is given by $\cos^{-1}(\vec{k}_0 \cdot \vec{k}_1)$ and $\bar{p}_1$ is the projection of $\vec{p}_1$ on the scattering vector.

Now let a second scattering of type A_2 occur from an electron with momentum $\vec{p}_2$ at $\vec{\rho}_2$, a distance $l_1' \le l_1$ from $\vec{\rho}_1$. The photon then traverses a distance l_2 from $\vec{\rho}_2$ to the cylinder boundary along $\vec{k}_2$, the new scattering direction, and is observed leaving the sample with energy E_2 and direction $\vec{k}_p$ in the laboratory frame of reference. E_2 is determined by E_1, θ_2, and $\vec{p}_2$ according to Eq. (1).

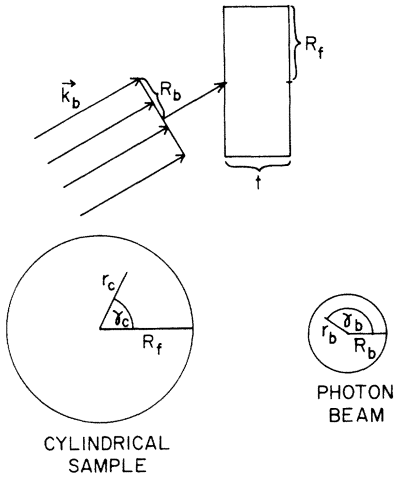

FIG. 1. Model of a Compton scattering experiment.

If we let $\vec{k}_p$ assume all possible values, then $\vec{k}_2$ also takes on all possible values, and we have the total probability of observing all such double scattering events:

$$P_T^{(A_1,A_2)}(\vec{k}_0, E_0, R_b, R_f, t) = \int_0^{2\pi} d\gamma_b \frac{1}{2\pi} \int_0^{R_b} dr_b \frac{2r_b}{R_b^2} \int_0^{l_0(\vec{k}_0,\vec{\rho}_0)} dl_0'\, \mu_0 e^{-\mu_0 l_0'} f_{0,A_1} \times \int d\Omega_1 \int d^3p_1\, |\chi(\vec{p}_1)|^2 \left(\frac{d\sigma}{d\Omega_1}\right)_{A_1} \int_0^{l_1(\vec{k}_1,\vec{\rho}_1)} dl_1'\, \mu_1 e^{-\mu_1 l_1'} f_{1,A_2} \times \int d\Omega_2 \int d^3p_2 |\chi(\vec{p}_2)|^2 \left(\frac{d\sigma}{d\Omega_2}\right)_{A_2} \times e^{-\mu_2 l_2(\vec{k}_2,\vec{\rho}_2)}, \qquad (2)$$

where $|\chi(\vec{p}_i)|^2$ is the electronic momentum distribution in the sample. The differential cross sections $(d\sigma/d\Omega_i)_{A_i}$ will in general depend upon the initial and final photon energies E_{i-1} and E_i, polarizations $\vec{\epsilon}_{i-1}$ and $\vec{\epsilon}_i$, and directions $\vec{k}_{i-1}$ and $\vec{k}_i$, as well as upon the electronic momenta $\vec{p}_i$.[11] As in Paper I we can change variables and replace the integration over Ω_2 in Eq. (2) by an integration over Ω_p, where $\vec{k}_2$ and $(d\sigma/d\Omega_2)_{A_2}$ are now expressed as functions of $\vec{k}_p$ and $\vec{k}_1$.

In an actual experiment one generally observes only those photons which exit the sample with $\vec{k}_p$ in some given range of solid angle $\Omega_p^{\rm exp}$. The probability of observing (A_1, A_2) events under such circumstances is (for brevity we suppress the arguments R_b, R_f, t)

$$P_T^{(A_1,A_2)}(\vec{k}_0, E_0, \Omega_p^{\rm exp}) = \int_0^{2\pi} d\gamma_b \frac{1}{2\pi} \int_0^{R_b} dr_b \frac{2r_b}{R_b^2} \int_0^{l_0(\vec{k}_0,\vec{\rho}_0)} dl_0' \, \mu_0 e^{-\mu_0 l_0'} f_{0,A_1} \times \int d\Omega_1 \int d^3p_1 \, |\chi(\vec{p}_1)|^2 \left(\frac{d\sigma}{d\Omega_1}\right)_{A_1} \int_0^{l_1(\vec{k}_1,\vec{\rho}_1)} dl_1' \, \mu_1 e^{-\mu_1 l_1'} f_{1,A_2} \times \int_{\Omega_p^{\rm exp}} d\Omega_p \int d^3p_2 |\chi(\vec{p}_2)|^2 \left(\frac{d\sigma}{d\Omega_2}\right)_{A_2} \times e^{-\mu_2 l_2(\vec{k}_2,\vec{\rho}_2)}. \quad (3)$$

Equation (3) is easily generalized to any order n of scattering. Let $\vec{A}^n$ be an ordered n-tuple of scattering types $(A_1, A_2, \ldots, A_n)$. Then

$$P_T^{(\vec{A}^n)}(\vec{k}_0, E_0, \Omega_p^{\rm exp}) = \int_0^{2\pi} d\gamma_b \frac{1}{2\pi} \int_0^{R_b} dr_b \frac{2r_b}{R_b^2} \int_0^{l_0(\vec{k}_0,\vec{\rho}_0)} dl_0' \mu_0 e^{-\mu_0 l_0'} \times \prod_{i=1}^{n-1} \left[f_{i-1,A_i} \int d\Omega_i \int d^3p_i |\chi(\vec{p}_i)|^2 \left(\frac{d\sigma}{d\Omega_i}\right)_{A_i} \int_0^{l_i(\vec{k}_i,\vec{\rho}_i)} dl_i' \, \mu_i e^{-\mu_i l_i'} \right] \times f_{n-1,A_n} \int_{\Omega_p^{\rm exp}} d\Omega_p \int d^3p_n |\chi(\vec{p}_n)|^2 \left(\frac{d\sigma}{d\Omega_n}\right)_{A_n} e^{-\mu_n l_n(\vec{k}_n,\vec{\rho}_n)}, \quad (4)$$

where now $\vec{k}_n$ and $(d\sigma/d\Omega_n)_{A_n}$ are expressed as functions of $\vec{k}_p$ and $\vec{k}_0, \vec{k}_1, \ldots, \vec{k}_{n-1}$. A change of variable similar to that carried out in Paper II will yield an energy profile for $\vec{A}^n$-type scattering.

We can take account of the spread in initial photon energies and directions by integrating over the normalized distribution $\bar{\Delta}(\vec{k}_0, E_0)$:

$$P_T^{(\vec{A}^n)}(\Omega_p^{\rm exp}) = \int_{\text{all } \vec{k}_0} d\vec{k}_0 \int_{E_0^{\min}}^{E_0^{\max}} dE_0 \, \bar{\Delta}(\vec{k}_0, E_0) P_T^{(\vec{A}^n)}(\vec{k}_0, E_0, \Omega_p^{\rm exp}). \quad (5)$$

The *total* amount of n-scattered radiation is then obtained by summing the $P_T^{(\vec{A}^n)}$ over all nonidentical permutations of scattering sequences $(\vec{A}^n)_J$:

$$P_T^n(\Omega_p^{\rm exp}) = \sum_J P_T^{(\vec{A}^n)_J}(\Omega_p^{\rm exp}). \quad (6)$$

For double scattering $(n=2)$, the possible $(\vec{A}^n)_J$ are (C,C), (C,R), (R,C), and (R,R).

Exact analytic calculation of the quantities defined above seems at best remote. Standard numerical integration techniques, such as those employed in Paper II, are generally useful only for single integrals. Numerical integration of the multidimensional integrals and complicated integrands involved here is best approached by the powerful and flexible Monte Carlo technique.

II. MONTE CARLO–GENERAL CONSIDERATIONS

A. Focus of the present work

For the purpose of our Monte Carlo calculations, we now wish to limit the very general experimental model described by Eqs. (4) and (5). We introduce the following restrictions:

(a) $\vec{k}_b = (0,0,1)$, i.e., the photon beam is incident at right angles to the cylinder face.

(b) $\bar{\Delta}(\vec{k}_0, E_0) = \delta(\vec{k}_0 - \vec{k}_b)\delta(E_0 - \bar{E}_0)$; the photon beam is perfectly collimated and monochromatic.

(c) $I(p_i) = \delta(0)$; the electrons are stationary.

(d) $(d\sigma/d\Omega_i)_{A_i}$ is given by either the Thomson or the Klein-Nishina differential cross section.

Under these conditions, Eqs. (4)–(6) for single scattering reduce essentially to Eq. (10b) of Paper I, while for double scattering we have

$$P_T^{(A_1,A_2)}(R_b,t,E_0,R_f,\Omega_p^{\exp})$$

$$= \int_0^{2\pi} d\gamma_b \frac{1}{2\pi} \int_0^{R_b} dr_b \frac{2r_b}{R_b^2} \int_0^t dz\, \mu_0 e^{-\mu_0 z} f_{A_1} \int_0^{\pi} d\theta_1 \sin\theta_1 \int_0^{2\pi} d\varphi_1 \left(\frac{d\sigma}{d\Omega_1}\right)_{A_1} \int_0^{l_1} dl_1' \mu_1 e^{-\mu_1 l_1'} f_{A_2}$$

$$\times \int_{\theta_{p_1}}^{\theta_{p_2}} d\theta_p \sin\theta_p$$

$$\times \int_0^{2\pi} d\varphi_p \left(\frac{d\sigma}{d\Omega_2}\right)_{A_2} e^{-\mu_2 l_2}, \tag{7}$$

where the solid angle $\Omega_p^{\exp}$ lies in the range $\theta_{p_1} \le \theta_p \le \theta_{p_2}$. Generalization to higher-order scattering is obvious.

In Paper I we obtained analytic expressions for the total probabilities and angular distributions of single and double scattering under certain additional restrictions:

(I-1) $(R_f - R_b)/t \gg 1$.

(I-2) $(d\sigma/d\Omega)_{A_i} = (3/16\pi)(\cos^2\theta_i + 1)$, the normalized Thomson cross section.

(I-3) μ is independent of energy, i.e., $\mu_0 = \mu_1 = \mu_2$.

(I-4) Higher-order scattering could not be calculated.

(I-5) Electrons are stationary.

In Paper II we were able to calculate energy profiles of single- and double-scattered radiation by a single numerical integration assuming only:

(II-1) $(R_f - R_b)/t \gg 1$.

(II-2) Electrons are stationary.

We also investigated the effects on energy profiles of elastic-inelastic scattering sequences, the use of other forms of the cross section, and, in somewhat less detail, the variation of μ with energy.

The primary purpose of this paper is to use Monte Carlo techniques to assess the validity of some of the assumptions of Papers I and II; to determine when and how badly they fail.

A full investigation via Monte Carlo of the behavior of total probabilities, angular distributions, and energy profiles when one or a combination of the assumptions of Papers I and II are relaxed would be a monumental and expensive task. Therefore only a limited set of calculations, aimed at qualitatively exploring the limitations of those assumptions, have been performed. Before discussing the results of these calculations we first give a brief discussion of our Monte Carlo programs and some of the techniques which they employ. A more detailed presentation may be found in Ref. 12.

B. Computational approach (Ref. 13)

The application of Monte Carlo techniques to the problem of multiple-Compton scattering may be viewed in either of two alternative, but compatible ways. Williams and Halonen[6,7] have emphasized the mathematical aspects of the problem, i.e., that Monte Carlo is a computational technique for estimating the value of a multiple integral such as that in Eq. (7). They have combined this approach with the use of variance reduction techniques to improve the accuracy and efficiency of their calculations considerably. We, on the other hand, focus our attention, like Felsteiner *et al.*,[3-5] on the more physical features; i.e., we view the Monte Carlo calculation as a means of simulating and tabulating the actual photon trajectories. We have, however, utilized a number of techniques similar to those of Williams and Halonen in order to make our calculations considerably more efficient than those described in Refs. 3–5.

Our Monte Carlo calculations proceed as follows. A large number m of photons are sampled or simulated by the computer. Each photon has the same initial energy E_0 and initial direction $\vec{k}_0 = (0,0,1)$. A point of entry on the cylinder face is chosen randomly within the photon beam, and then a point of first scattering is chosen by inverting[13] the exponential probability distribution $P(z) = 1 - e^{-\mu z}$. Since, especially for thin samples, the probability of the first scattering occurring within the sample may be small, the efficiency of the program is increased by "forcing" the first collision to occur within the sample, i.e., by employing the modified probability distribution

$$\tilde{P}(z) = (1 - e^{-\mu z})/(1 - e^{-\mu t}), \tag{8}$$

where t is the sample thickness. Each photon is then given a "weight" of $1 - e^{-\mu t}$ instead of 1. Looked at another way, each photon is "partitioned" into two portions: one with weight $e^{-\mu t}$ which scatters outside the sample (and which

we need not consider further), and a second portion of weight $1 - e^{-\mu t}$ whose fate we now follow.

At the point of scattering, a new direction $\vec{k}_1$ is chosen for the photon by applying the rejection method[13] to the probability distribution determined by the appropriate differential cross section. The new energy of the Compton scattered photon is calculated from Eq. (1) and, if appropriate, the attenuation coefficient in the exponential distribution is changed to reflect this new energy.

The point of the next scattering $\vec{\rho}_2$ must now be chosen. In previously reported Monte Carlo calculations, the point is chosen by inverting the unmodified exponential distribution, Eq. (8). The point $\vec{\rho}_2$ is now tested to see if it lies inside or outside the sample. If outside, the energy and total scattering angle are tabulated as described below. If the photon is still within the sample, the procedure is iterated beginning with the choice of a new scattering angle.

In some applications we wish to study many orders of scattering or a particular order of scattering within a small range of observation angles θ_p, e.g., double scattering at $167° \pm 2°$. In such cases, we have been able to greatly improve the efficiency of the calculation. We force all collisions but the last to occur inside the sample using the modified distribution (9) with t replaced by l_n, the distance from the point of collision to the sample boundary along the scattering direction. The last collision is forced to occur outside the sample. On the last collision, the range of scattering directions which will cause the photon to emerge within the desired observation region is calculated. The scattering direction is then chosen from the differential cross section modified in such a way as to force the photon into this range. In this manner, *all* photons are forced to be "useful" and the large statistical uncertainties found in some earlier Monte Carlo studies[3] are reduced.

In the angular-distribution studies, the cosines x_p of the primary scattering angles range from -1 to 1. For each multiplicity of scattering this range is divided into 40 equally spaced channels. When a photon escapes the sample as described above, its weight is added to the appropriate channel according to the value of x_p. In this way, for each order of scattering, estimates are obtained of 40 integrals similar to that of Eq. (7). For example, for single Compton scattering, let m_i be the number of single-scattered photons escaping the sample with x_p in the interval $[x_i, x_{i+1})$. Then

$$P_i^{\mathrm{MC}} = \frac{m_i}{m} = P_T^{(C)}(R_b, t, E_0, R_f, x_i x_{i+1})$$
$$= \int_0^{2\pi} d\gamma_b \frac{1}{2\pi} \int_0^{R_b} dr_b \frac{2r_b}{R_b^2} \int_0^{t} dz\, \mu_0 e^{-\mu_0 z} f_C \int_{x_i}^{x_{i+1}} dx_p \int_0^{2\pi} d\varphi_p \left(\frac{d\sigma}{d\Omega_1}\right)_C e^{-\mu_1 t_1} \tag{9}$$

Since $x_{i+1} - x_i = 0.05$, we use the mean-value theorem to approximate

$$\left.\frac{\partial P^{(C)}(x_p)}{\partial x_p}\right|_{x_p = x_i + 0.025} \approx \left(\frac{1}{0.05}\right) P_i^{\mathrm{MC}}. \tag{10}$$

Calculation of the angular distributions of once- and twice-scattered photons for one sample thickness using 10^3 photons requires approximately 16 sec of computing time on the Brandeis PDP-10 computer. If n is the multiplicity of scattering being considered and m the number of photons sampled, then the computing time t is given roughly by

$$t = Cmn, \tag{11}$$

where $C = 2.5 \times 10^{-6}$ h.

III ANGULAR DISTRIBUTIONS AND TOTAL PROBABILITIES

A. Error analysis and overlap with analytic work

As a check on our computer program and as a means of estimating the errors to be expected from the Monte Carlo calculations, the program was run with parameters chosen in accordance with the assumptions of Paper I. In Table I we compare the Monte Carlo results obtained by sampling varying numbers of photons with the values calculated analytically. Here and in the following sections, the fractional difference δ between a quantity q and its Monte Carlo estimate q_{MC} is defined as

$$\delta = \left|(q_{\mathrm{MC}} - q)/q\right|. \tag{12}$$

One expects δ to decrease roughly as the reciprocal of the square root of M, the number of photons sampled. Table I bears out this expectation. We see in Fig. 2 that even with only 25 000 sample points, excellent agreement is obtained between the analytic and Monte Carlo double-scattered angular distributions.

B. Klein-Nishina cross section

In Paper I we were unable to derive analytic angular distributions using the Klein-Nishina cross section averaged over polarizations:

TABLE I. Calculated values of total probabilities and angular distributions of single and double scattering from an infinite-radius cylinder of optical thickness $\omega = 1.0$.

	Single scattering		Double scattering		Angular
	P_1	δ_1	P_2	δ_2	distribution[a]
Analytic	0.2715	...	0.1382	...	...
Monte Carlo, 10^3 photons	0.2589	0.464×10^{-1}	0.1418	0.260×10^{-1}	0.233
Monte Carlo, 10^4 photons	0.2702	0.479×10^{-2}	0.1370	0.868×10^{-2}	0.669×10^{-1}
Monte Carlo, 10^5 photons	0.2717	0.737×10^{-3}	0.1382	0.000	0.254×10^{-1}
Monte Carlo, 10^6 photons	0.2718	0.110×10^{-2}	0.1383	0.724×10^{-3}	0.784×10^{-2}

[a] Double scattering. Average of fractional difference δ_i for the ith exit channel averaged over the 40 exit channels.

$$\left(\frac{d\sigma}{d\Omega}\right)_{KN} = \left(\frac{r_0^2}{2}\right)\left(\frac{E_1}{E_0}\right)^2\left(\frac{E_1}{E_0}+\frac{E_0}{E_1}-\sin^2\theta\right), \qquad (13)$$

where θ is the angle of scattering. E_1 is related to E_0 by the Compton equation (1). For $E_0 \ll 1$ or for elastic scattering ($E_1 = E_0$), Eq. (13) reduces to the Thomson cross section.

The angular distributions of single- and double-scattered photons were calculated by the Monte Carlo program under the assumptions of Paper I, except that Eq. (13) was employed in place of the Thomson cross section. Figure 3 shows that the differences between the Thomson and Klein-Nishina results become quite significant for the higher-energy γ rays presently used in some experiments. At the lower x-ray energies (e.g., Mo $K\alpha$, $E_0 = 0.017$ MeV), the Thomson and Klein-Nishina results are nearly indistinguishable. As discussed in Paper I, the "randomizing effect" of the scattering causes differences due to the use of different cross sections to decrease as the order of scattering increases. All differences found between the various angular distributions may be explained qualitatively by the "Klein-Nishina asymmetry effect": the fact that unlike the symmetric Thomson cross section, the Klein-Nishina expression causes relatively more photons to be scattered forward than backward, and this asymmetry increases with increasing photon energy.

In Table II, we compare the total probabilities of single, double, and triple scattering calculated with the Thomson and Klein-Nishina cross sections. For single scattering use of the Klein-Nishina expression makes little difference for samples with $\omega \lesssim 1.0$. For thicker samples we have

$$P_1^{Th}(\omega) > P_1^{Mo\ K\alpha}(\omega) > P_1^{Am}(\omega) > P_1^{Te}(\omega). \qquad (14)$$

The intuitions developed in Paper I and the Klein-Nishina asymmetry effect easily rationalize this trend.

For thin samples, the probability of a second scattering is nearly independent of whether a photon is first scattered forward or backward. As ω increases, however, the probability of scattering again becomes greater for a forward-scattered than for a backward-scattered photon, since the path length through the sample will in general be greater for the former than for the latter. Hence, single scattering of higher-energy photons will be reduced and double scattering enhanced, since these photons will be preferentially forward scattered according to Eq. (13). We therefore also expect that the inequalities in Eq. (14) will be reversed for double scattering and indeed they are from $\omega \sim 0.5$ to $\omega \sim 2.0$. For thicker samples, triple scattering becomes significant, and our simple analysis breaks down. Higher-order scattering appears far more difficult to analyze, though the table suggests that it may be relatively insensitive to E_0 and/or to the form of the differential

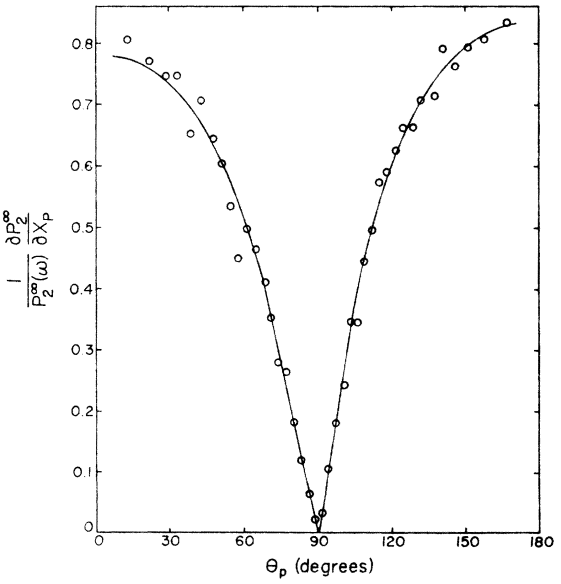

FIG. 2. Normalized angular distributions of double scattering with $\omega = 1.0$, $R_f = 10^4$. Solid line is analytic calculation; circles are Monte Carlo results with a sample of 25 000 photons.

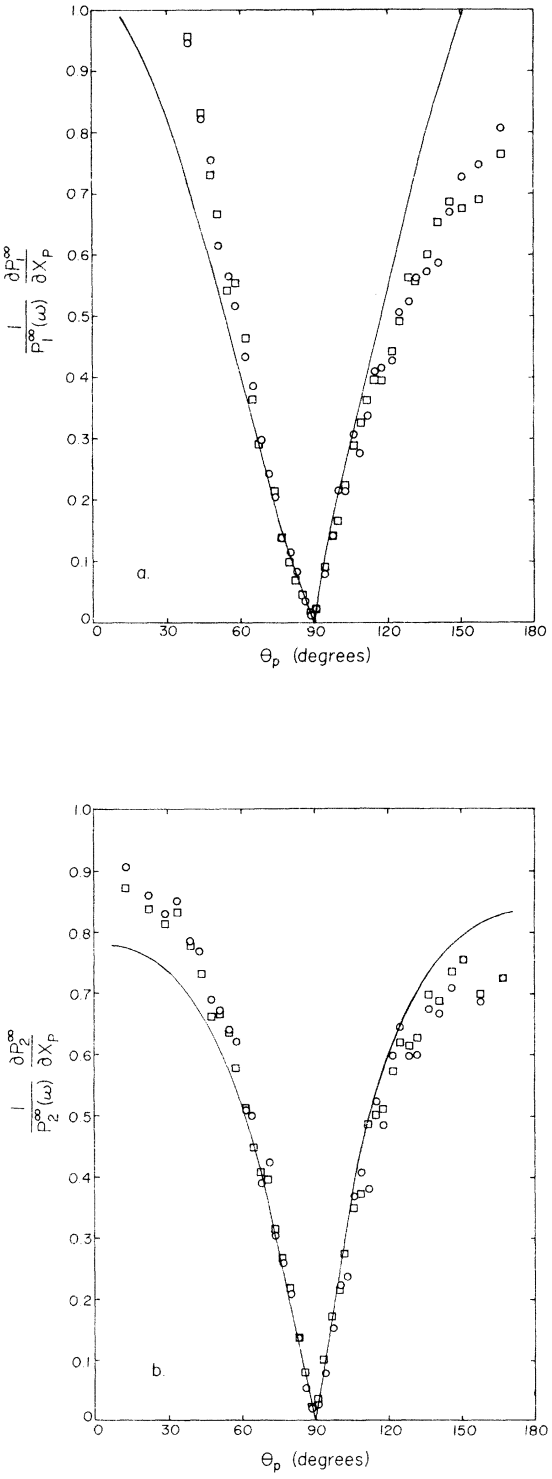

FIG. 3. Normalized angular distributions with $\omega = 1.0$, $R_f = 10^4$, $E_0 = 0.0159$ MeV (Te γ rays). Solid line is analytic Thomson result; circles are Monte Carlo Klein-Nishina calculations. (a) Single scattering; (b) double scattering.

cross section. The randomizing effect referred to above seems crucial here.

The angular distributions show significant variation with E_0 when the Klein-Nishina cross section is employed. For single scattering and θ_p close to 180°, the asymmetry effect predicts the observed trend, a set of inequalities parallel to those of Eq. (14). For higher-order scattering and/or smaller scattering angles, the effects of sample geometry and of asymmetry in the cross section appear to counteract one another, and the net result is extremely complex. In a number of cases, angular distributions for Mo $K\alpha$ x rays (0.017 MeV) resemble those for Te γ rays (0.159 MeV) more closely than either resembles the distribution for Am γ rays (0.059 MeV).

C. Polarization-dependent Thomson cross section

The Thomson cross section for polarized photons is[14]

$$\frac{d\sigma}{d\Omega} = r_0^2 \sin^2\Theta , \tag{15}$$

where Θ is the angle between the initial polarization vector $\vec{\epsilon}_0$ and the final direction $\vec{k}_1$ of the photon. In Paper I, we showed that the single-scattered angular distribution was identical whether Eq. (15) or its average over initial polarizations

$$\frac{d\sigma}{d\Omega} = \frac{r_0^2}{2}(1+\cos^2\theta) \tag{16}$$

is employed. We were not able to calculate the double-scattered angular distribution analytically using Eq. (15), but a Monte Carlo calculation of this quantity is quite straightforward.

The program previously described is augmented by assigning each photon a random initial polarization uniformly distributed in the x-y plane. Equation (15) is used to generate the probability distribution of scattering directions. The new polarization $\vec{\epsilon}_1$ is coplanar with $\vec{\epsilon}_0$ and $\vec{k}_1$, and orthogonal to $\vec{k}_1$. According to Eq. (15), a photon is most likely to scatter in a direction perpendicular to $\vec{\epsilon}_0$.

In Fig. 4 we see that unlike the single-scattered angular distribution, $(\partial P_2/\partial x)$ is significantly affected by the use of Eq. (15) in place of Eq. (16); the inclusion of polarization results in a sizable enhancement of scattering near 0° and 180° at the expense of scattering near 90°. Photons which scatter first with $\theta_1 = \pi/2$ must have new polarization $\vec{k}_1$ in the x-y plane. Owing to the infinite-radius geometry, these photons *must* scatter a second time, and this scattering is most likely to occur in a direction perpendicular to $\vec{\epsilon}_1$, i.e., in the z direction. This accounts for the observed increase in $(\partial P_2/\partial x_p)$ for $|x_p| \sim 1$.

TABLE II. Thomson and Kelin-Nishina scattering probabilities for infinite-radius cylinder.

ω	Type	Thomson [a]	Klein-Nishina Mo $K\alpha$ x rays	Klein-Nishina Am γ rays	Klein-Nishina Te γ rays
0.001	Single	0.9964×10^{-3}	0.9966×10^{-3}	0.9963×10^{-3}	0.9990×10^{-3}
	Double	0.311×10^{-5}	0.291×10^{-5}	0.316×10^{-5}	0.281×10^{-5}
	Triple	$\sim10^{-7}$	$\sim10^{-7}$	$\sim10^{-7}$	$\sim10^{-7}$
0.01	Single	0.9725×10^{-2}	0.9731×10^{-2}	0.9724×10^{-2}	0.9736×10^{-2}
	Double	0.219×10^{-3}	0.213×10^{-3}	0.220×10^{-3}	0.209×10^{-3}
	Triple	0.622×10^{-5}	0.595×10^{-5}	0.646×10^{-5}	0.607×10^{-5}
0.05	Single	0.4479×10^{-1}	0.4479×10^{-1}	0.4472×10^{-1}	0.4485×10^{-1}
	Double	0.3633×10^{-2}	0.3584×10^{-2}	0.3632×10^{-2}	0.3510×10^{-2}
	Triple	0.358×10^{-3}	0.361×10^{-3}	0.373×10^{-3}	0.363×10^{-3}
0.10	Single	0.8186×10^{-1}	0.8198×10^{-1}	0.8188×10^{-1}	0.8218×10^{-1}
	Double	0.1106×10^{-1}	0.1098×10^{-1}	0.1105×10^{-1}	0.1079×10^{-1}
	Triple	0.183×10^{-2}	0.183×10^{-2}	0.186×10^{-2}	0.182×10^{-2}
0.50	Single	0.2347	0.2344	0.2343	0.2350
	Double	0.8734×10^{-1}	0.8775×10^{-1}	0.879×10^{-1}	0.8830×10^{-1}
	Triple	0.388×10^{-1}	0.389×10^{-1}	0.389×10^{-1}	0.385×10^{-1}
1.00	Single	0.2715	0.2710(0.2696) [b]	0.2681	0.2665(0.2666) [b]
	Double	0.1382	0.1379(0.1393) [b]	0.1410	0.1423(0.1436) [b]
	Triple	0.847×10^{-1}	0.842×10^{-1}	0.844×10^{-1}	0.846×10^{-1}
2.00	Single	0.2369	0.2318	0.2255	0.2162
	Double	0.1437	0.1447	0.1484	0.1513
	Triple	0.106	0.107	0.109	0.111
5.00	Single	0.1738	0.1656	0.1531	0.1327
	Double	0.0996	0.0986	0.1010	0.0962
	Triple	0.0741	0.0739	0.0743	0.0745

[a] Single and double scattering values are analytic (Ref. 1); triple scattering values calculated by Monte Carlo program under the assumptions of Paper I.

[b] Results of two different Monte Carlo runs (25000 photons each) are given as an illustration of the statistical uncertainties.

As the above argument suggests, the effect of using the polarized cross section, Eq. (15), is found to be somewhat smaller, though still significant for finite radius cylinders. For the infinite-radius cylinder of Fig. 4 with $\omega = 1.0$ the average fractional difference between the polarized and unpolarized $(\partial P_2/\partial x_p)$ is about 0.15. For the same sample thickness, but with $R_f = 1.0$, $R_b = 0.5$, this difference decreases to about 0.13. An infinite-radius cylinder with $\omega = 0.001$ gives an average fractional difference of 0.25, again supporting the conclusion of Paper I that differences in cross section are most influential at small thickness.

D. Higher-order scattering

The analytic procedures of Paper I were incapable of treating scattering of order three and higher. With the forcing techniques discussed in Sec. II B, the Monte Carlo approach is easily adapted to the study of higher-order scattering. In Table III we present Monte Carlo calculations of the total probabilities of n scattering under the assumptions of Paper I. Included for comparison are the corresponding analytic results for $n = 1$ and 2. As n increases, the $P_n^\infty(\omega_{max})$ decreases with n.

We also find from Table III that for a given ω, the ratio $P_{n+1}^\infty(\omega)/P_n^\infty(\omega)$ appears to be a constant independent of n, as long as n is greater than some minimum value $n(\omega)$. For relatively thin samples $n(\omega)$ is 1, and it increases with ω. The limiting ratio of the $(n+1)$th- to nth-order scattering is a decreasing function of ω. These observations may be rationalized as follows. After a certain number of scatterings, $n(\omega)$, a typical photon finds itself "in the middle" of the sample. Clearly $n(\omega)$ will increase with ω. At this point, the ratio $P_{n+1}^\infty(\omega)/P_n^\infty(\omega)$ or, equivalently, the ratio of the probability of escape to the probability of further scattering depends only upon the distance to the sample faces, i.e., upon ω, and not upon the past history of the photon. The chance of another scattering and hence the ratio of $n+1$ to n scattering will obviously increase with ω. The above argument should

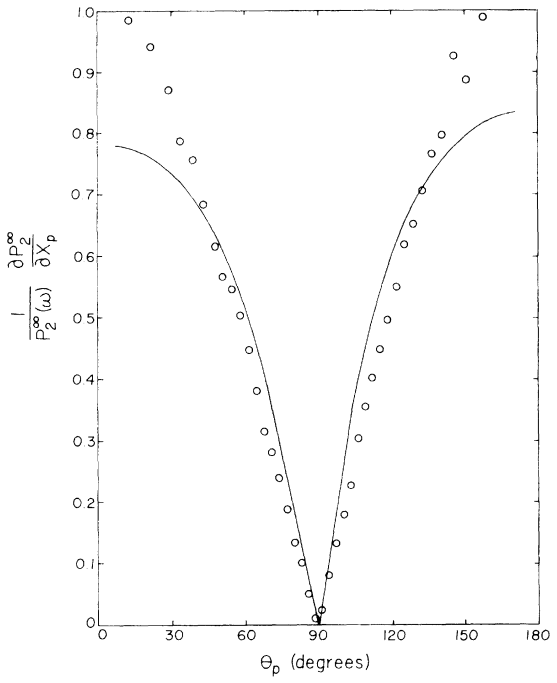

FIG. 4. Normalized angular distributions for double scattering with $\omega = 1.0$, $R_f = 10^4$. Solid line is analytic result for unpolarized Thomson cross section. Circles are Monte Carlo calculations using polarized Thomson cross section.

also be applicable to finite samples, though the ratio should depend upon R_f (but not R_b) as well as upon ω. These results suggest that *for most samples, determination of the probabilities of relatively low orders of scattering may suffice for an accurate estimate of higher-order scattering probabilities.*

In the infinite-cylinder model higher-order scattering is non-negligible even for $\omega = 0.1$. However, it was shown in Paper I that this model gives an upper limit for higher-order scattering. For finite samples, triple and higher-order scattering will be considerably reduced by the escape of photons through the sides of the cylinder. Also, photoelectric absorption will decrease the value of $P_n(\omega)$ by a factor of roughly f_C^n. For a light molecule like water, f_C varies from about 0.1–0.2 at x-ray energies to 0.88–0.98 for γ rays.

E. Finite geometry

One of the assumptions made in deriving the results of Papers I and II was that

$$B \equiv (R_f - R_b)/t \gg 1 . \tag{17}$$

In this section we investigate multiple scattering when this condition does not hold, and we obtain estimates of the values of ω, μR_b, and μR_f for which the results of Papers I and II are applicable.

TABLE III. Monte Carlo calculation of total probability of nth-order scattering from an infinite-radius cylinder.

Optical thickness ω	$P_1^\infty(\omega)$ [a]		$P_2^\infty(\omega)$ [a]		$P_3^\infty(\omega)$	$P_4^\infty(\omega)$
0.1	0.8200×10^{-1}	0.8186×10^{-1}	0.1097×10^{-1}	0.1106×10^{-1}	0.1829×10^{-2}	0.3120×10^{-3}
0.5	0.2352	0.2342	0.8694×10^{-1}	0.8734×10^{-1}	0.3880×10^{-1}	0.1769×10^{-1}
1.0	0.2718	0.2715	0.1383	0.1382	0.8465×10^{-1}	0.5137×10^{-1}
2.0	0.2389	0.2369	0.1422	0.1437	0.1057	0.8112×10^{-1}
3.0	0.2002	0.2012	0.1233	0.1228	0.9448×10^{-1}	0.7656×10^{-1}
4.0	0.1823	0.1823	0.1094	0.1077	0.8129×10^{-1}	0.6575×10^{-1}
5.0	0.1771	0.1738	0.1004	0.9962×10^{-1}	0.7413×10^{-1}	0.6034×10^{-1}
10.0	0.1724	0.1677	0.9125×10^{-1}	0.9243×10^{-1}	0.6757×10^{-1}	0.5093×10^{-1}
Optical thickness ω	$P_5^\infty(\omega)$	$P_6^\infty(\omega)$	$P_7^\infty(\omega)$	$P_8^\infty(\omega)$	$P_9^\infty(\omega)$	$P_{10}^\infty(\omega)$
0.1	0.5194×10^{-4}	0.1021×10^{-4}	0.164×10^{-5}	0.28×10^{-6}	0.5×10^{-7}	0.1×10^{-7}
0.5	0.8014×10^{-2}	0.3696×10^{-2}	0.1672×10^{-2}	0.7728×10^{-3}	0.3451×10^{-3}	0.1648×10^{-3}
1.0	0.3245×10^{-1}	0.2012×10^{-1}	0.1269×10^{-1}	0.7926×10^{-3}	0.4839×10^{-2}	0.3025×10^{-2}
2.0	0.6321×10^{-1}	0.4975×10^{-1}	0.3923×10^{-1}	0.3120×10^{-1}	0.2465×10^{-1}	0.1884×10^{-1}
3.0	0.6414×10^{-1}	0.5441×10^{-1}	0.4643×10^{-1}	0.4016×10^{-1}	0.3471×10^{-1}	0.2998×10^{-1}
4.0	0.5742×10^{-1}	0.4853×10^{-1}	0.4395×10^{-1}	0.3952×10^{-1}	0.3552×10^{-1}	0.3231×10^{-1}
5.0	0.5091×10^{-1}	0.4266×10^{-1}	0.3801×10^{-1}	0.3372×10^{-1}	0.3006×10^{-1}	0.2805×10^{-1}
10.0	0.4035×10^{-1}	0.3492×10^{-1}	0.2804×10^{-1}	0.2410×10^{-1}	0.2130×10^{-1}	0.1854×10^{-1}

[a] Second column is analytic result (Ref. 1).

For simplicity, we set $\mu = f_C = 1$ here; thus $\omega = t$ and only Compton events are considered.

The Monte Carlo program was used to calculate angular distributions and total probabilities of once- and twice-scattered radiation for a wide range of t, R_b, and R_f. We find that, as predicted in Paper I, the analytic infinite-cylinder total probability of single scattering $P_1^\infty(\omega)$ is a lower bound to the corresponding probability $P_1(\omega)$ for finite samples. This behavior is seen in Fig. 5. We also find that for thin samples ($\omega \lesssim 0.5$)$P_1(\omega)$ is quite close to $P_1^\infty(\omega)$, for essentially all R_f and R_b, since nearly all photons escape through the sample faces. For thicker samples, the possibility of escape through the sides becomes important, and $P_1(\omega)$ begins to depend strongly upon the radii of both the sample and the beam. As Fig. 5 shows, a small sample radius results in a $P_1(\omega)$ curve which rises monotonically to an asymptotic limit whose value depends upon R_b. For thicker samples, $P_1(\omega)$ rises to a maximum, then declines to its asymptotic value. Generally, the probability of single scattering is almost independent of beam radius for $R_b < 0.5R_f$, but then increases sharply with R_b for larger beam radii. We attribute this somewhat unexpected behavior to the increase in the probability of escape through the cylinder sides as R_b approaches R_f.

If $R_f \geq 5.0$, the $P_1(\omega)$ curve is nearly indistinguishable from $P_1^\infty(\omega)$. Even when $R_f = t = 5.0$, so that B in Eq. (17) is only 0.98, $P_1(\omega)$ differs by less than 1% from the infinite-cylinder value.[15] We thus conclude (a) that Eq. (15) provides a sufficient but not necessary condition for the applicability of the results of Paper I, and (b) that a path length of 5.0 or more is "effectively infinite." Physically, the validity of our analytic results depends upon the assumption that photons escape predominantly through the faces of the cylinder rather than through the sides. A less stringent but more meaningful parameter than B of Eq. (17) may then be

$$B' = (R_f - \tfrac{2}{3}R_b)/t\,, \tag{18}$$

where $\frac{2}{3}R_b$ is the average distance of photons in the beam from the sample axis. We find that in general a value of B' greater than or equal than 3.0 is sufficient to assure that $P_1(\omega)$ will differ from $P_1^\infty(\omega)$ by no more than 2%.

Higher-order scattering in finite cylinders is somewhat more difficult to characterize than single scattering, because for $n > 1$ it is no longer true that $P_n^\infty(\omega)$ provides a lower bound for the finite-cylinder n-scattering probability $P_n(\omega)$. We do find, however, that B' of Eq. (18) remains a useful parameter for characterizing the approach to infinite-cylinder behavior and that higher-order scattering from samples with $R_f \geq 5.0$ differs little from the infinite-cylinder limits for total probabilities and angular distributions. Figure 6 illustrates the change in the double-scattered angular distribution as we increase the radius of a finite sample until with $\mu R_f = 5$, we approach the infinite-radius limit.

Although $P_n^\infty(\omega)$ is not in general a lower bound for $P_n(\omega)$, our Monte Carlo results indicate that for each multiplicity of scattering $n \leq 5$ there exists a critical sample thickness ω_n, which depends upon R_b and R_f, such that

$$P_n^\infty(\omega) \leq P_n(\omega) \quad \text{if } \omega \geq \omega_n\,,$$

i.e., $P_n^\infty(\omega)$ *is* a lower bound for sufficiently thick samples and all $n' \leq n$. This critical thickness ω_n is an increasing function of n. We note, however, that for n sufficiently large, $P_n(\omega)$ must be less than $P_n^\infty(\omega)$ regardless of sample thickness, because essentially all of the photons will have escaped the finite-radius sample after $n-1$ scat-

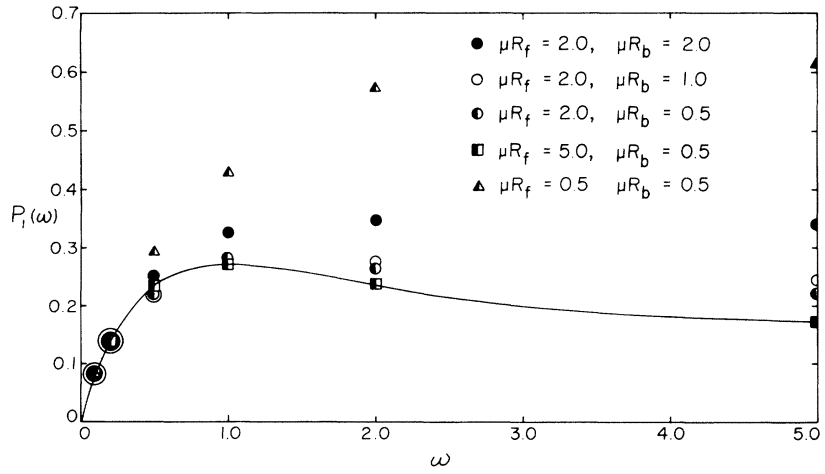

FIG. 5. Total probability of single scattering for same finite-radius cylinders. Solid line is analytic infinite-cylinder value.

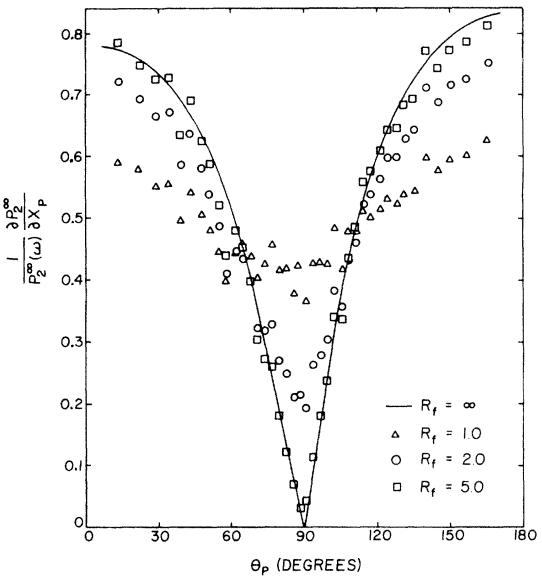

FIG. 6. Normalized angular distribution for double scattering from a finite cylinder with $\mu R_b = 0.5$, $\omega = \mu t = 1.0$.

terings.

Differences between double-scattered angular distributions calculated using the polarization-dependent Thomson cross section [Eq. (15)] and the polarization-averaged cross section [Eq. (16)] are smaller in finite- than in infinite-radius cylinders. However, for the Klein-Nishina cross section and Te γ radiation, the average difference (about 9%) between the double-scattered angular distributions and the corresponding values obtained using Eq. (16) appears to be independent of sample radius.

IV. ENERGY PROFILES

A. General considerations

In Paper II a variable ϵ was defined as the sum of the cosines of the Compton scattering angles. It was shown that energy profiles could immediately be derived from ϵ profiles, since the energy of a photon which has undergone n scatterings, j of them Compton, is

$$E_n(\epsilon) = \frac{E_0}{1 + E_0(j - \sum_{i=1}^{j}\cos\theta_i)} = \frac{E_0}{1 + E_0(j - \epsilon)}. \qquad (19)$$

In this section, ϵ profiles are presented for two cases not treated in Paper II: for double scattering from finite cylinders using the Thomson cross section first averaged over polarizations [Eq. (16)], then for polarized radiation, Eq. (15). Double-scattered profiles for polarization-averaged Thomson and Klein-Nishina scattering from finite-radius cylinders were calculated and compared in Paper II.

Unlike the continuous ϵ profiles $K_{CC}(\epsilon, x_p)$ of Paper II, the Monte Carlo data presented here are discrete in nature. That is, our Monte Carlo results are the values of integrals of the form

$$\Delta K_{CC}(\epsilon_m) = \int_{\epsilon_m}^{\epsilon_{m+1}} d\epsilon \int_{x_{p_1}}^{x_{p_2}} dx_p K_{CC}(\epsilon, x_p). \qquad (20)$$

We define a normalized quantity $\tilde{\Delta}K_{CC}(\epsilon_m)$ such that

$$\sum_m \tilde{\Delta}K_{CC}(\epsilon_m) = 1$$

by dividing each $\Delta K_{CC}(\epsilon_m)$ by the total scattering probability for the range (x_{p_1}, x_{p_2}).

A typical computing time on the Brandeis PDP-10 for an ϵ profile derived from 10^4 double-scattered photons is about 2.5 min. Using an expression of the form of Eq. (11), we find that $C \approx 5 \times 10^{-6}$ h, in agreement with Eq. (11) for double scattering ($n = 2$).

B. ϵ profiles for finite cylinders

In Fig. 7 we show the normalized ϵ profiles for double scattering from an infinite- and a finite-radius cylinder for the angular interval $165^\circ \leq \theta_p \leq 169^\circ$ calculated with our Monte Carlo program. The Thomson cross section averaged over photon polarizations has been employed. Note that the sharp features found for the infinite-radius cylinder in Paper II have disappeared as a result of the integration in Eq. (20). The two normalized profiles are remarkably similar, the average fractional difference being about 0.06. Of course, the absolute profiles differ considerably more, since the total probability (sum over ϵ) for the infinite cylinder is 0.1143, while for the finite cylinder the value is 0.0999.

In Fig. 8 we again observe a striking similarity between the double-scattered profiles calculated

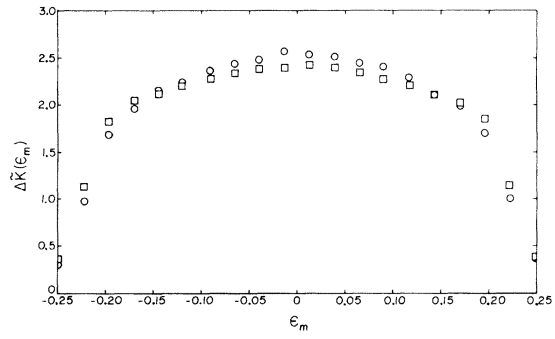

FIG. 7. Normalized ϵ profiles for double scattering from a finite cylinder with $\mu R_b = 0.5$, $\omega = \mu t = 1.0$. Polarization-averaged Thomson cross section. □, $R_f = 10^3$ (infinite cylinder), 10^6 photons; ○, $R_f = 1.0$, 10^5 photons.

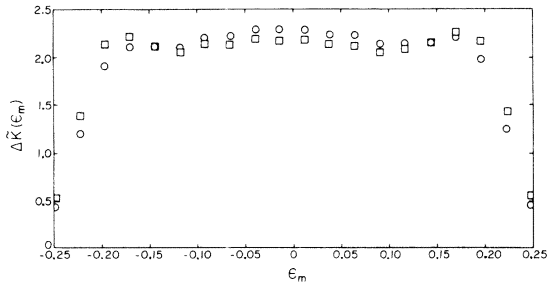

FIG. 8. Same as Fig. 8, but with polarization-dependent Thomson cross section and 10^5 photons in each profile.

from finite and infinite cylinders, this time with the polarization-dependent Thomson cross section. The average fractional difference δ[Eq. (12)] is 0.07. We do note, however, a significant difference between the polarized and polarization-averaged calculations, with a δ value of 0.14. Thus the value of R_f appears to affect the shapes of the ϵ profiles far less than the form of the cross section.

Since the *shapes* of the double-scattered profiles appear to be relatively independent of sample radius, differences between finite- and infinite-sample profiles will arise primarily from differences in the magnitudes of the double scattering probabilities. Therefore, the criteria established in Sec. III for the validity of the infinite-cylinder total probabilities and angular distributions will be applicable to energy profiles as well.

V. COMPARISON WITH OTHER WORK

Since our Monte Carlo calculations have been aimed primarily at a qualitative understanding of the behavior of multiple scattering in situations not at present susceptible to analytic calculation, no detailed comparison with Monte Carlo calculations of other workers will be undertaken.

The variation of total multiple scattering with sample thickness in finite cylinders agrees well with that observed by Felsteiner and Pattison.[5] Their finding that multiple scattering from samples with large attenuation coefficients (e.g., Al or Cu irradiated by Mo $K\alpha$ x rays) reaches "infinite limits" for very small sample thickness is confirmed by our results. The flattening of the angular distribution which we observe with increasing order of scattering has also been noted in an earlier work by Felsteiner *et al.*[3]

Our energy profiles are considerably more refined in terms of statistical accuracy than those presented by Felsteiner *et al.*[3] for stationary electrons in water. This refinement is made possible by the forcing routines described earlier. Our results also agree qualitatively with the energy profiles for aluminum calculated by Halonen *et al.*[7]

VI. SUMMARY AND CONCLUSIONS

We have found that total probabilities, angular distributions, and energy profiles of multiple-scattered radiation can be significantly different for finite-radius cylinders than for the infinite-radius cylinder model used in Papers I and II. Depending upon the order of scattering, the quantity in question, and the sample and beam dimensions, it has been found that a sample can be considered "effectively infinite" even when $\mu R_f \sim 2.0$. When $\mu R_f \sim 5.0$ the sample is almost always effectively infinite.

The use of either the Klein-Nishina cross section averaged over polarizations or the polarization-dependent Thomson cross section may result in significant departures from the multiple scattering behavior calculated with the polarization averaged Thomson cross section. However, the qualitative conclusions from our earlier analytic work are still found to be valid. In addition, the effect of employing the Klein-Nishina cross section for x-ray scattering is relatively small.

ACKNOWLEDGMENTS

We are extremely grateful to Dr. B. G. Williams for a number of illuminating discussions on multiple scattering and Monte Carlo techniques. We also thank Dr. Williams and Dr. V. Halonen for communicating their results prior to publication. Acknowledgment is made to the donors of the Petroleum Research Fund, administered by the American Chemical Society, for support of this research.

---

*Work supported by the Camille and Henry Dreyfus Foundation.

[1]Paper I: A. C. Tanner and I. R. Epstein, Phys. Rev. A 13, 335 (1976).

[2]Paper II: A. C. Tanner and I. R. Epstein, preceding paper, Phys. Rev. A 14, 313 (1976).

[3]J. Felsteiner, P. Pattison, and M. Cooper, Philos. Mag. 30, 537 (1974).

[4]P. Pattison, S. Manninen, J. Felsteiner, and M. Cooper, Philos. Mag. 30, 973 (1974).

[5]J. Felsteiner and P. Pattison, Nucl. Instrum. Methods 124, 449 (1975).

[6]B. G. Williams and V. Halonen, Phys. Fennica 10, 5 (1975).
[7]V. Halonen, B. G. Williams, and T. Paakkari, Phys. Fennica (to be published).
[8]V. Kourganoff, *Basic Methods in Transfer Problems* (Clarendon, Oxford, England, 1952).
[9]O. I. Leipunskii, B. V. Novozhilov, and V. N. Sakharov, *Propagation of Gamma Quanta in Matter* (Pergamon, New York, 1975).
[10]At higher energies a variety of additional processes, such as pair production, begin to occur. See, e.g., J. H. Hubbell, *Photon Cross Sections, Attenuation Coefficients, and Energy Absorption Coefficients From* 10 *keV to* 100 *GeV*, NSRDS-NBS N35, Circ. No. 29 (U. S. GPO, Washington, D. C., 1969).
[11]P. Eisenberger and P. M. Platzman, Phys. Rev. A 2, 415 (1970).
[12]A. C. Tanner, Ph.D. thesis (Brandeis University, 1975) (unpublished).
[13]For detailed treatments of the principles of Monte Carlo, see *The Monte Carlo Method*, edited by Y. A. Shrieder, (Pergamon, New York, 1966); J. M. Hammersley and D. C. Handscomb, *Monte Carlo Methods* (Methuen, London, 1964).
[14]J. D. Jackson, *Classical Electrodynamics* (Wiley, New York, 1962), p. 489.
[15]We also recall from Paper I that both $P_1^{\infty}(\omega)$ and $P_2^{\infty}(\omega)$ are within 10% of their asymptotic values when $\omega = 5.0$.